View metadata, citation and similar papers at core.ac.uk

brought to you by CORE

provided by IntechOpen

We are IntechOpen, the world's leading publisher of Open Access books Built by scientists, for scientists

4,800
Open access books available

122,000
International authors and editors

135M
Downloads

154
Countries delivered to

Our authors are among the
TOP 1%
most cited scientists

12.2%
Contributors from top 500 universities

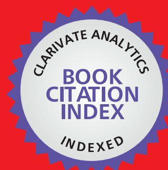

WEB OF SCIENCE™

Selection of our books indexed in the Book Citation Index in Web of Science™ Core Collection (BKCI)

Interested in publishing with us?
Contact book.department@intechopen.com

Numbers displayed above are based on latest data collected.
For more information visit www.intechopen.com

12

In-Situ Analysis of Optoelectronic Properties of Semiconductor Nanostructures and Defects in Transmission Electron Microscopes

Yutaka Ohno[1], Ichiro Yonenega[1] and Seiji Takeda[2]
[1]*Institute for Materials Research, Tohoku University*
[2]*Osaka University*
Japan

1. Introduction

A wide variety of optoelectronic devices such as photovoltaic (including solar cells and photo detectors), photoemitting (including lasers) and photocatalytic devices have been developed for more than five decades. The physical nature of such devices, especially operated with visible and near-infrared light, is electronic transitions between pairs of energy levels, typically in semiconductors. In addition to the conduction band and the valence band, defect levels, i.e., localized energy levels associated with nanostructures and lattice defects, are responsible for the electronic transitions. Various kinds of nanostructures can be fabricated, spontaneously or artificially, inside and onto semiconductors. Also, lattice defects, such as point defects (including vacancies, interstitials, dopant and impurity atoms) and extended defects (including grain boundaries, stacking faults, dislocations, and point defect clusters), can be introduced, inevitably or accidentally, during crystal growth and device fabrication processes. Therefore, in order to fabricate optoelectronic devices with advanced and ultimate functions, the structural properties of semiconductor nanostructures and defects, as well as their optoelectronic properties such as the possible presence of defect levels, should be understood with a high spatial resolution simultaneously with a high spectral resolution.

Optical measurements such as luminescence and photoabsorption spectroscopy are powerful techniques to determine defect levels. Since the spectral resolution is higher than the order of 10^{-3} eV, this techniques are useful to study the energy levels in the low energy range between the band edges of semiconductors (of the order of 10^{0} eV at most), which dominate the optoelectronic properties of the device products made of the materials. Therefore, when the measurements are performed in a transmission electron microscope (TEM), such as near-field optical measurements in a TEM (Ohno, 2010a), we can examine the optoelectronic properties simultaneously with the structural properties in small regions observed in-situ with the TEM.

With an extremely high spectral resolution in comparison with the other spectroscopic techniques in TEM, such as energy dispersive x-ray spectroscopy (e.g., Terauchi et al, 2010) and electron energy-loss spectroscopy (e.g., Kikkawa et al, 2007) with a resolution less than about 10^{-1} eV, the optical measurements in TEM enable us to assess in detail defect levels in

small regions. It is interesting to note that we can examine in-situ the optoelectronic and structural properties of nanostructures and defects *inside* a material, which properties are affected by the surrounding material and are not determined in-situ by the optical measurements in scanning probe microscopes, such as scanning near-field optical microscopy. As the continuing miniaturization and integration of optoelectronic devices, the optical measurements in TEM have been established as an indispensable micro-characterization technique. In this chapter, principles of the optical measurements in TEM, i.e., cathodoluminescence (CL) spectroscopy and transmission electron microscopy under light illumination are briefly summarized, and the resent analysis of some semiconductors for optoelectronic devices are reviewed.

2. Principles of the optical measurements in TEM

2.1 CL spectroscopy in TEM

CL is a phenomenon of light emission induced by electron irradiation. CL light is emitted from a region in which electrons are irradiated, and the optical parameters, such as the photon energy, intensity and polarization, vary depending on the electronic structure in the region. Therefore, CL spectroscopy performed in a TEM enables us to examine the electronic structure simultaneously with the atomic structure in small regions observed in-situ with the TEM, where electrons are irradiated. For example, the structural and compositional variation, as well as the defect concentration and distribution, can be determined. Also, the electronic properties such as defect levels and their carrier capture cross sections, which are associated with the carrier lifetime and diffusion length, can be analyzed. In this subsection, the principles underlying the generation and interpretation of CL signals are summarized. The detailed descriptions of the principles including the pioneer work in 1978 (Petroff et al, 1978) are provided in a review (Yacobi and Holt, 1990).

2.1.1 Spatial resolution of CL measurements

Electrons irradiated into a material can undergo elastic and inelastic scattering. The irradiated material is excited via inelastic electron scattering, and this excitation results in the formation of x-rays, Auger electrons, secondary electrons, electron-hole pairs, and so forth. CL lights are emitted via the recombination of electron-hole pairs. The spatial resolution of CL measurements is, therefore, determined by the distribution of electron-hole pairs.

When electrons are irradiated into a material, each electron changes its direction via an elastic scattering, and it reduces its kinetic energy via an inelastic scattering. As a result of the scattering processes, the original trajectories of the electrons are randomized. For a thin solid material through which most incident electrons can transmit, used as a specimen in a TEM, the shape of the electron penetration range (a so called generation volume) is conical and the radius of a generation volume, which is the maximum at the electron exit surface, is determined (Goldstein, 1979). Electrons and holes are generated inside a generation volume, via some electron-electron interactions. They can diffuse in a material, and the distribution of electron-hole pairs is dominated by the diffusion of minority carriers. The stationary density of minority carriers at a position $\mathbf{r}$, $\Delta n(\mathbf{r})$ obeys the differential equation of continuity, $\mathrm{div}[\mathrm{grad}\, \Delta n(\mathbf{r})]D - \Delta n(\mathbf{r})/\tau(\mathbf{r}) + g(\mathbf{r}) = 0$, in which D is the diffusion constant for minority carriers, τ is the mean recombination lifetime, and g is the generation rate of electron-hole pairs. The distribution of minority carriers has been discussed theoretically

(e.g., Everhart & Hoff, 1971, Donolato & Venturi, 1982), and the range in which minority carriers exist is expected to be twice as large as a generation volume at most, for thin materials. Therefore, the spatial resolution of CL measurements can be approximated to the maximum diameter of a generation volume. The typical resolution is the order of 10^2 nm.

2.1.2 CL spectroscopy and analysis

CL lights are emitted via various radiative electronic transitions. One transition is the recombination between an electron in the conduction band and a hole in the valence band (a band-to-band transition), which is typical in direct gap semiconductors at high temperatures. At a temperature T at which kT (k is the Boltzmann factor) is smaller than the binding energy for free excitons, the excitonic level for the excitons is formed just below the conduction band edge and the decay of the excitons (the free exciton transition between the excitonic level and the valence band) results in a CL emission. When a defect exists, it may induce donor and/or acceptor levels. Electrons and holes generated by electron irradiation are trapped at the levels, and CL lights may be emitted via a donor-to-valence band transition, a conduction band-to-acceptor transition, and a donor-to-acceptor transition. They are the typical transitions in indirect gap semiconductors at high temperatures. Similar to the case of free excitons, the excitonic levels bound to a donor and an acceptor are formed at low temperatures and CL lights may be emitted via the decay of the excitons (bound exciton transitions). Also, when an impurity with incomplete inner shells (such as a rare earth ion or a transition metal) exists, its excitation and radiative deexcitation (an inner shell transition) results in a CL emission. Detailed recombination processes are reviewed, for example, by Henderson & Imbusch (Henderson & Imbusch, 1989) for inner shell transitions, and by Yu & Cardona (Yu & Cardona, 2001) for the other transitions.

The photon energy of a CL light emitted via a transition is written as $\Delta E+\delta$, in which ΔE corresponds to the energy difference between the energy levels concerning the transition. δ is a positive value for a donor-to-acceptor transition (Yu & Cardona, 2001), and it is zero for the other transitions. CL energy measurements have been used to assess energy levels in a small volume, which are connected to the structure including defects and composition in the volume.

When the number N of nanostructures or defects of the same kind, with the cross section for radiative recombination of σ, exist in a small volume, the number of photons emitted from the volume per a unit time is proportional to $N\sigma$. CL intensity measurements have been applied to assess the density of point defects acting as radiative recombination center (e.g., Graham et al, 1994, Mitsui et al, 1996) and those acting as non-radiative one (e.g., Ohno et al, 1999, Ohno & Takeda, 1996). Also, the techniques have been used to assess the carrier dynamics such as excited carrier paths towards the lower energy states (e.g., Akiba et al, 2004, Merano et al, 2005, Sonderegger et al, 2006), as well as carrier lifetimes.

Some extended defects such as dislocations (Yamamoto et al, 1984, Mitsui & Yamamoto, 1997), twins (Ohno et al, 2007b), platelets (Ohno, 2005a) and strains induced by a uniaxial stress (Wang et al, 1993, Ohno, 2005b), as well as low-dimensional nanostructures such as nanowires (Ishikawa et al, 2008, Yamamoto et al, 2006), quantum wells (Ohno, 2005a) and superlattices (Ohno & Takeda, 2002, Ohno et al, 2007b), form anisotropic defect levels, and electronic transitions via the levels result in the emission of polarized CL lights. CL polarization analyses have helped us to assess quantitatively the atomistic structures of such nanostructures and defects.

2.1.3 CL imaging and analysis

A CL image (or a CL intensity map) is obtained by detecting the CL intensity as an electron beam scans a raster over a specimen. When there is a microstructure, such as a defect, in which the cross section for radiative or non-radiative recombination differs from that in the surrounding homogeneous material, contrast arises in CL images. For example, the spatial distribution of defects in degraded devices (e.g., Sieber et al, 1993, Cheng et al, 1995, Bonard et al, 1998) have been determined.
CL contrast due to a defect varies depending on the atomistic structure, size and location of the defect. Among them, effects of dislocations on CL contrast have been determined theoretically (e.g., Jakubowicz, 1986, Schreiber & Hildebrandt, 1994, Holt & Napchan, 1994), and the radiative and non-radiative lifetime and diffusion length for minority carriers around a dislocation have been assessed.

2.2 Electron microscopy under light illumination

CL spectroscopy in TEM is a useful technique to determine defect levels of nanostructures and defects acting as radiative recombination center. However, a defect level acting as non-radiative recombination center is, in general, difficult to assess. Also, it is difficult to examine the process of an electronic excitation (i.e., an electronic transition from an energy level to a higher one) via a defect level, since various kinds of electronic excitaitions take place simultaneously during the irradiation of electrons whose energy is much higher than the band gap energy. In order to determine such electronic transitions with a high spatial resolution, transmission electron microscopy under light illumination has been used, since the pioneer work in 1984 (Suzuki et al, 1984). In this subsection, the principles underlying the electronic transitions induced by light illumination are summarized.

2.2.1 Electronic transitions due to light illumination

Unlike electronic transitions due to electron irradiation, induced via an interaction between electrons, electronic transitions due to the illumination of a light, especially in visible and near-infrared region, are mainly induced via an interction of photons with electrons. For a photo-induced electronic transition between two energy levels, the transition rate is high when the photon energy of the illuminating light is close to the energy difference between the levels (in a resonant photo-excitation condition), according to the Fermi's golden rule. Therefore, by choosing a proper photon energy which corresponds to the energy difference between a defect level and an another level, we can selectively determine the defect level. When the technique is applied in TEM, it is useful to determine the nanostructures and defects whose atomistic structures vary under photo-excitation conditions.
Under the illumination of a light with a proper photon energy, electron-hole pairs can be generated. Therefore, the spatial resolution of optical measurements with photo-excitation is approximated to the diameter of the generation volume, similar to CL measurements. Since a light beam almost goes straight inside a thin material, the resolution is approximated to the diameter of the beam. In case of the illumination of a far-field light in TEM with a conventional optical system, such as an optical fiber (Suzuki et al, 1984, Yoshida et al, 2004), optical lens (Ohno & Takeda, 1995), and parabolic mirror (Ohno, 2010a), the resolution is much less than 10^3 nm due to the diffraction limit of light. The spatial resolution beyond the limit, higher than 10^2 nm, is acheived in a TEM with a near-field light probe (Ohno, 2010a).

2.2.2 In-situ photo-excitation in TEM and analysis

Transmission electron microscopy under light illumination has been used to study in-situ photo-induced structural variations such as the dislocation motion related to photo-plasticity (Suzuki et al, 1984) and degradations in photoemitters (Ohno, 2005b, 2010a, Ohno et al, 2009b); the glide of dislocations under light illumination is observabed in-situ. Photocatalytic reactions in catalysts are also observable in-situ, and a photo-induced decomposition (Yoshida et al, 2004), structural transformation (Yoshida et al, 2006), and nucleation of nanostructures (Yoshida et al, 2007) are observed in a photocatalytic system. Such a structural variation is induced via a photo-induced electronic excitation, and depends on the photon energy, intensity and polarization of the illuminating light. A defect level related to the photo-excitation can be estimated with a proper photon energy, since the degree of the structural variation is the maximum when the photon energy is close to the energy difference between the defect level and an another level (Ohno, 2005b, Ohno et al, 2009b, Ohno, 2010a).
Semiconductors under light illumination can emit photoluminescence (PL) light, similar to CL, so as to release some of the photon energy absorbed from the illuminating light. PL spectroscopy has an advantage over CL spectroscopy when various kinds of nanostructures and defects coexist in a small region. A defect level of nanostructures or defects of the same kind can be determined selectively, since the emission efficiency is increased in a resonant photo-excitation condition in which the illuminating light is absorbed via the defect level. Also, Raman spectroscopy, by which the phonon structure of nanostructures and defects can be determined, is available under light illumination, in a resonant photo-excitation condition. PL and Raman spectroscopy with a far-field light is demonstrated in TEM (Ohno & Takeda, 1995, 1996, Ozaki et al, 1998, Ohno et al, 1999, Kohno et al, 2004, Ohno, 2010a).

2.2.3 In-situ photo-excitation systems in TEM

As a convenient system, an optical fiber is installed inside a TEM so that the end of the fiber is located near the area observed with the TEM (Suzuki et al, 1984, Yoshida et al, 2004). Even though the system is easily constructed in any TEMs, the spatial resolution is rather low; almost all areas on a TEM specimen are illuminated. Here a high resolution system for in-situ photo excitation is reviewed.
Figure 1 shows an apparatus for in-situ high-resolution optical measurements with a near-field light probe in a TEM (Ohno, 2010a). A metal tip is located close to the area observed with the TEM. The tip is then illuminated with a far-field light, and an intense near-field light is induced in the immediate vicinity of the tip apex, due to a surface enhanced effect (Inouye & Kawata, 1994).
In detail, a specimen in a TEM is illuminated with a laser light by using a parabolic mirror. The mirror is truncated so that it is inserted inside a small space in the TEM and the specimen is illuminated with an electron beam for TEM observation. A laser light is introduced into the TEM so that the optical pass is parallel to the rotation axis of the parabolic mirror, and the introduced light is focused onto the focal point of the mirror. With a CL technique (Ohno & Takeda, 1995), the focal point is set onto the area observed with the TEM. A specimen generally exhibits CL emission during TEM observation, and the CL light emitted from the observed area is detectable optically. Also, a laser light focused on a specimen is detectable. Each light is observed as a bright spot with an optical zoom microscope. By adjusting the location of the parabolic mirror so that the laser spot coincides to the CL spot, the laser light is precisely focused onto the area observed with the TEM. In order to form a near-field light, a metal tip is located on the observed area with a TEM-STM

holder (Figs. 1c and 1d). The tip is set in the side illumination configuration in which the tip axis is about normal to the optical pass of a laser light for inducing a near-field light. With the configuration, an intense near-field light can be induced at the tip apex, due to a *p*-polarization effect (Hayazawa et al, 2002).

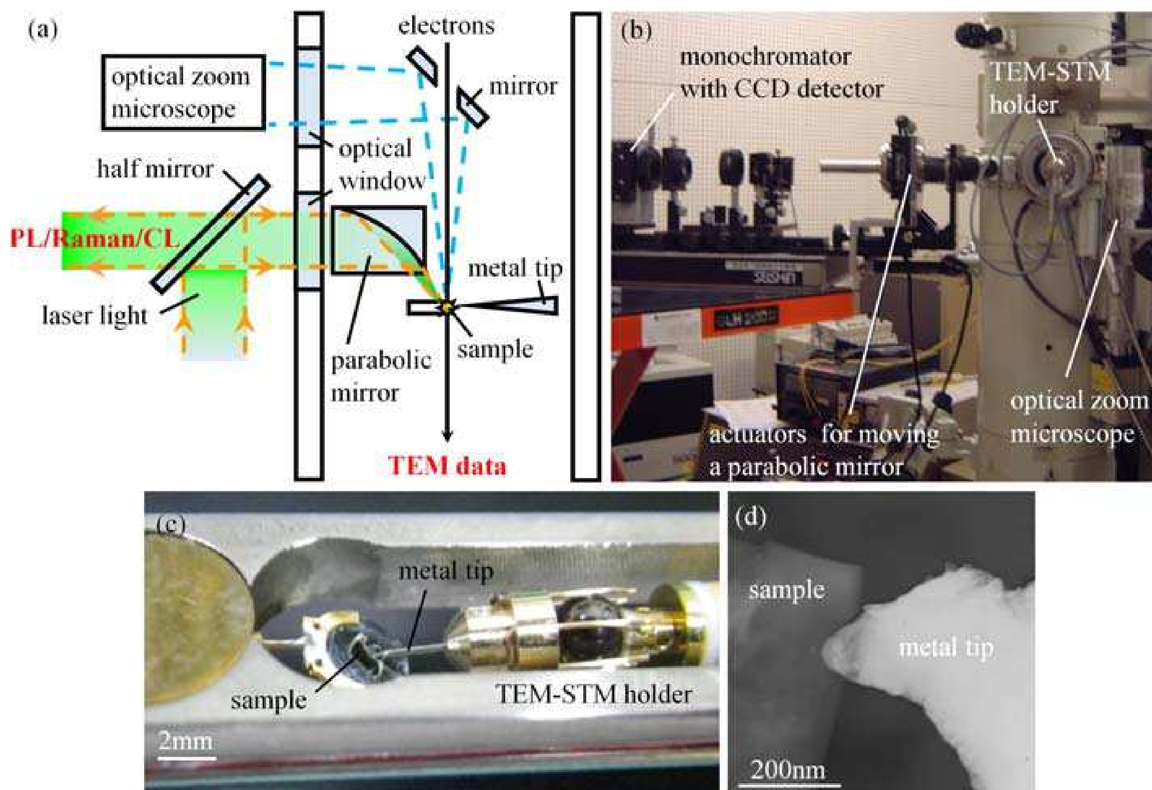

Fig. 1. (a) Schematic and (b) external views of an apparatus for in-situ near-field optical measurements in a TEM. (c) Optical and (d) TEM images of a specimen and a metal tip in a TEM-STM holder

3. Optoelectronic properties of semiconductor nanostructures and defects

3.1 Dislocations in wide gap semiconductors

Extended defects in semiconductors frequently affect the optoelectronic properties. Among them, dislocations are key topics for developing the relevant devices fabricated with wide gap semiconductors, such as GaN and ZnO, since they are inevitably introduced a high density of dislocations. In this subsection, the recent knowledge of the optoelectronic properties of dislocations, mainly revealed by in-situ optical measurements in a TEM, is reviewed. The properties in GaN, which is the pioneer of the commercial photoemitting device operated in the short wavelength range, are first summarized, and those in ZnO, which is attracting keen interest as a promising analog to GaN, are shown.

GaN and related materials have been applicated to short-wavelength optoelectronic devices since the successful fabrication of long-lifetime blue photoemitting diodes operated at room temperature (Nakamura et al, 1994). Due to the lack of a suitable growth substrate, there exist mismatches in lattice constant and in thermal expansion coefficient between a GaN epilayer and its substrate (e.g., sapphire or SiC), and the mismatches induce a high density (10^6-10^{10} cm^{-2}) of dislocations. However, the epilayer has a high efficiency of light emission.

It is well known that most dislocations act as non-radiative recombination center in III-V (e.g., Petroff et al, 1980, Hutchinson et al, 1984, Wang et al, 1992) and II-VI (e.g., Mitsui & Yamamoto, 1997, Mitsui et al, 1996) compound semiconductors, and the dislocations affect the device lifetimes even when the density is as low as 10^4 cm^{-2}. Therefore, the optical properties of dislocations in GaN have been a subject of controversy. Individual dislocations, grown-in (Yamamoto et al, 2003, Nakaji et al, 2005, Albrecht et al, 2008) and introduced intentionally (Albrecht et al, 2002, 2008), are examined in TEM, and the dislocations act as recombination-active centers. Actually, they often exhibit recombination-enhanced glide (Maeda et al, 1999). The dislocations lying on a basal plane (i.e., misfit dislocations) seem to be undissociated with the Burgers vector **b** of $1/3<11\underline{2}0>$ (Albrecht et al, 2002), even though they can be dissociated (Suzuki et al, 1994), presumably due to a high energy barrier for an undissociated dislocation to dissociate (Blumenau et al, 2003). Among the dislocations, 60° dislocations are proposed to act as radiative recombination center that emit a light with photon energy of 2.9 eV at low temperatures, while the other dislocations act as non-radiative recombination center (Albrecht et al, 2002). The screw dislocations have a small recombination activity in comparison with the edge dislocations (Yamamoto et al, 2003), even though their velocity for recombination-enhanced glide is faster in comparison with the edge dislocations (Maeda et al, 1999). Also, threading dislocations, i.e., dislocations lying on pyramidal planes with **b** = $1/3<11\underline{2}0>$ (Albrecht et al, 2008) and those on prismatic planes with **b** = $1/3<11\underline{2}0>$ or $1/3<11\underline{2}1>$ (Yamamoto et al, 2003), act as non-radiative recombination center. Even though the threading dislocations have a smaller recombination activity in comparison with the misfit dislocations (Yamamoto et al, 2003), they reduce overall luminescence intensities (Yonenaga et al, 2006). The diffusion length of minority carriers around a dislocation is estimated (Yamamoto et al, 2003, Nakaji et al, 2005, Ino & Yamamoto, 2008), and it is smaller in comparison with the other semiconductors; e.g., about 200 nm, 150 nm, and 60 nm, respectively, for non-doped, Mg-doped ($1x10^{17}$ cm^{-3}), and Si-doped ($3x10^{18}$ cm^{-3}) GaN, even at low temperatures. The estimated length is smaller than the nearest-neighbor distances of dislocations, and this would be a reason why GaN can tolerate a much higher dislocation density than in the other semiconductors.

Wide gap II-VI compound semiconductors had been expected to be the most promising materials for short-wavelength optoelectronic devices, but most researches were closed after the commercialization of GaN-based devices. However, there is a revival of interest in the materials because of their potential applications in optoelectronic devices employing excitonic effects in the short wavelength range, due to their large exciton binding energy, etc. Among them, ZnO has rapidly emerged as a promising analog to GaN, after the demonstration of the excitonic emission at elevated temperatures up to 550 K (Bagnall et al, 1998). Despite considerable success in optimizing the growth conditions and structural quality such as the fabrication of blue photoemitters (Tsukazaki et al, 2005), ZnO epilayers still contain a number of defects. The most characteristic defect, investigated with a TEM, is a high density (10^9−10^{11} cm^{-2}) of dislocations (e.g., Setiawan et al, 2004). In ZnO, dislocations are introduced with lower stress and are much mobile, in comparison with GaN (Yonenaga et al, 2008). The knowledge of the influence of dislocations is, therefore, required for the practical use of this material.

In order to determine the effects of dislocations on the optoelectronic properties, an arbitrary number (10^9-10^{10} cm^{-2}) of dislocations on a basal plane are introduced in wurtzite ZnO single-crystals, at elevated temperatures (923-1123 K) comparable to the typical temperatures for the fabrication of ZnO-based devices, by compressive deformation (Ohno

et al, 2008a). The dislocations seem to be undissociated with **b** = a/3<11$\underline{2}$0>, even though they can be dissociated (Suzuki et al, 1994), similar to wurtzite GaN (Suzuki & Takeuchi, 1999, Albrecht et al, 2002). Most dislocations are of mixed type including 60° dislocations, and screw and edge dislocations also exist. Macroscopic PL measurements reveal that, unlike wurtzite GaN, the introduction of the dislocations do not influence all the emission bands existing in as-grown specimens (Fig. 2a). Also, additional emission bands, with photon energies E_L of 3.100 and 3.345 eV at temperature of 11 K, as well as their LO phonon replicas (with the separation between the nearest-neighbor emission lines of 72 meV), are introduced (Fig. 2b). From the analysis of the thermal quenching processes, the depth of the defect level ΔE associated with the 3.100 eV emission and that with the 3.345 eV one are estimated to be 0.3 eV and 0.05 eV, respectively. Since the PL intensities increase with increasing dislocation density, the emission bands are associated with the dislocations introduced at elevated temperatures (Ohno et al, 2008b).

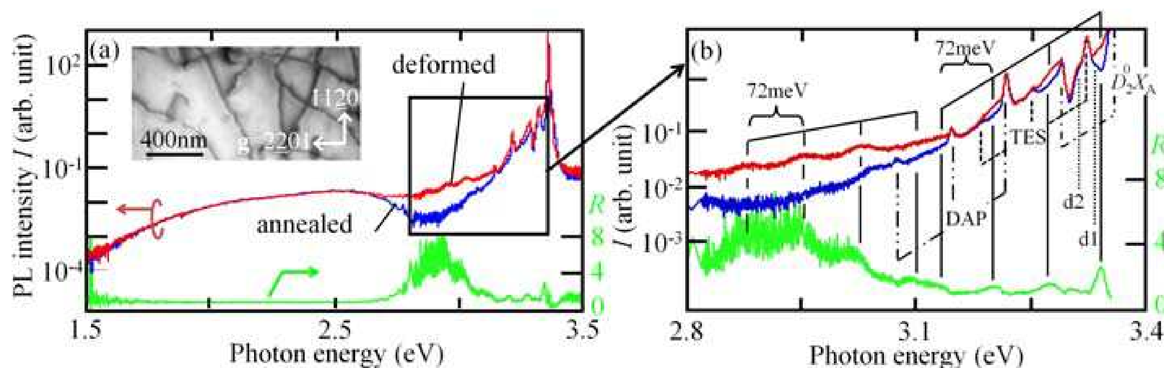

Fig. 2. PL intensity vs photon energy for a specimen deformed at 923 K (the red curve) or annealed at 923 K without stress (the blue curve). The ratio of those PL intensities, $R=I_{\text{deformed}}/I_{\text{annealed}}$, is also shown (the green curve). A part of (a) is magnified in (b). The inset in (a) shows a TEM image of dislocations in the deformed specimen. (Ohno et al, 2008b)

In-situ TEM observation with 80 keV electrons reveals that (Ohno et al, 2009b), screw and edge dislocations glide forming mixed dislocation segments when electrons are irradiated at temperature of 120 K, as well as at room temperature (Fig. 3). Effects of the point defects introduced by the irradiation is negligible, since the electron energy is much smaller than the threshold electron energy for displacement damage in ZnO (310 keV). The glide velocity for a dislocation is independent of irradiation temperature, and it increases with increasing electron flux. Therefore, the dislocations glide via an electron-hole recombination (Maeda et al, 2000), and the screw and edge dislocations act as non-radiative recombination center. The glide velocity for a screw dislocation is more than 10^{1} times larger in comparison with an edge dislocation. Those properties are similar to wurtzite GaN (Maeda et al, 1999).

In order to determine the optoelectronic properties of each individual dislocation, the recombination-enhanced glide is determined in detail by TEM observation under the illumination of a light, in the energy range of 2.25-2.92 eV, at temperature of 120K (Ohno et al, 2009b). A screw dislocation glides when a light with photon energy around 2.5 eV is illuminated (Fig. 4). Since the estimated energy is smaller than the band gap energy E_g (about 3.4 eV at 120 K) and is larger than the activation energy of about 1 eV for thermal dislocation glide (Yonenaga et al, 2008), electrons and holes would be recombined at a defect level associated with the dislocation, similar to the case of 90$^{\circ}\alpha$ partial dislocations in ZnSe (Ohno, 2005b). Namely, the depth of the defect level ΔE is about 0.9 eV (E_g–2.5 eV). Since the

recombination-enhanced glide of edge dislocations is not observed, their defect level would locate deeper than 1.15 eV (E_g–2.25 eV) and they might glide under the illumination of a light with the corresponding photon energy.

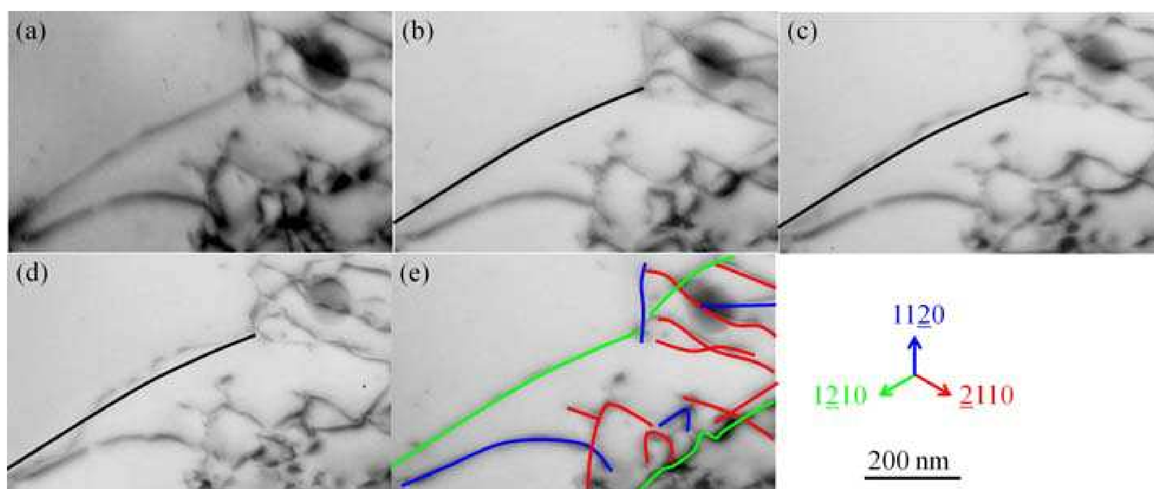

Fig. 3. Dislocation glide due to electron irradiation. The specimen is irradiated with electrons with flux of $5x10^{16}$ e mm^{-2} s^{-1} at room temperature for 3600 s (a to b). It is subsequently irradiated with flux of $5x10^{17}$ e mm^{-2} s^{-1} at room temperature for 900 s (b to c), then irradiated with the same flux at temperature of 120 K for 900 s (c to d). The black curves in b-d indicate the location of a screw dislocation before electron irradiation. (e) A schematic view of the dislocations with **b** = a/3[1$\underline{2}$10] (green curves), a/3[11$\underline{2}$0] (blue curves), and a/3[$\underline{2}$110] (red curves) in (a). (Ohno et al, 2009b). Copyright Wiley-VCH Verlag GmbH & Co. KGaA. Reproduced with permission

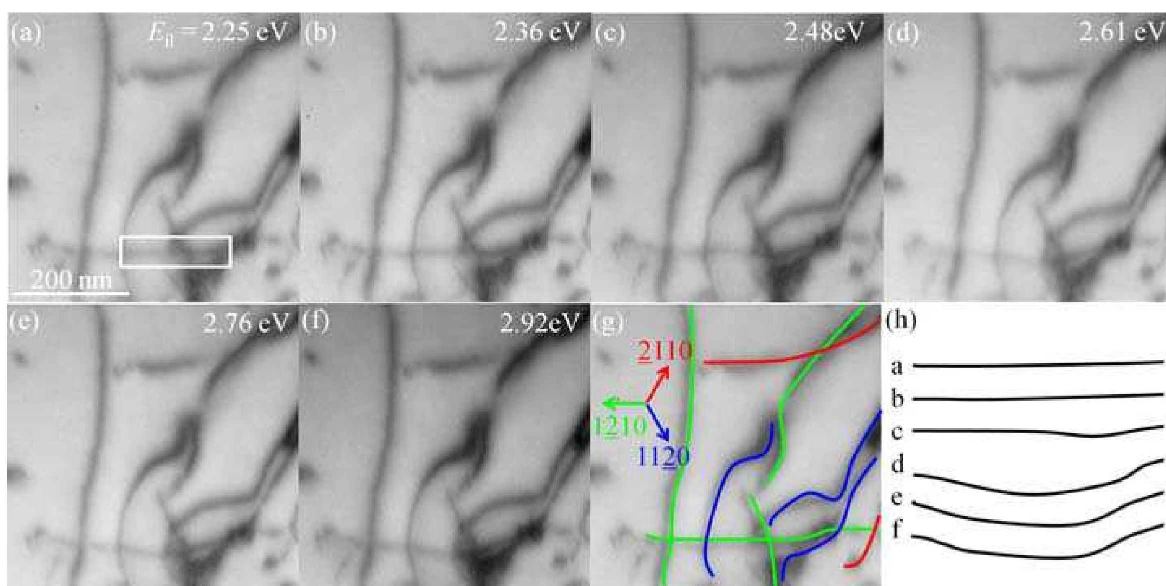

Fig. 4. (a – f) Dislocation glide due to light illumination. Dislocations are illuminated in turn with a light with the photon energy E_{il}. (g) A schematic view of the dislocations with **b** = a/3[1$\underline{2}$10] (green curves), a/3[11$\underline{2}$0] (blue curves), and a/3[$\underline{2}$110] (red curves) in (a). (h) Variation of the line shape of the screw dislocation in the squared area in (a) during light illumination. (Ohno et al, 2009b). Copyright Wiley-VCH Verlag GmbH & Co. KGaA. Reproduced with permission

The emission band peaking at 3.1 eV, due to a defect level of 0.3 eV depth associated with dislocations (Ohno et al, 2008b), is determined by CL spectroscopy (Ohno et al, 2009b). Since a CL light emitted from a dislocation is rather weak, CL lights are obtained from an area in which a number of dislocations exist (the total length of the dislocation lines of about 2×10^3 nm). The lights are collected after the light illumination with the same illumination sequence as in Fig. 4, and the intensity is unchanged during the illumination (Fig. 5). The intensity is also unchanged during electron irradiation (Fig. 6). Therefore, the emission is not influenced by the conversion of screw and edge dislocations into mixed dislocations, via their recombination-enhanced glide under light illumination or electron irradiation. Those results indicate that the origin of the emission band is neither the screw dislocations nor the edge ones.

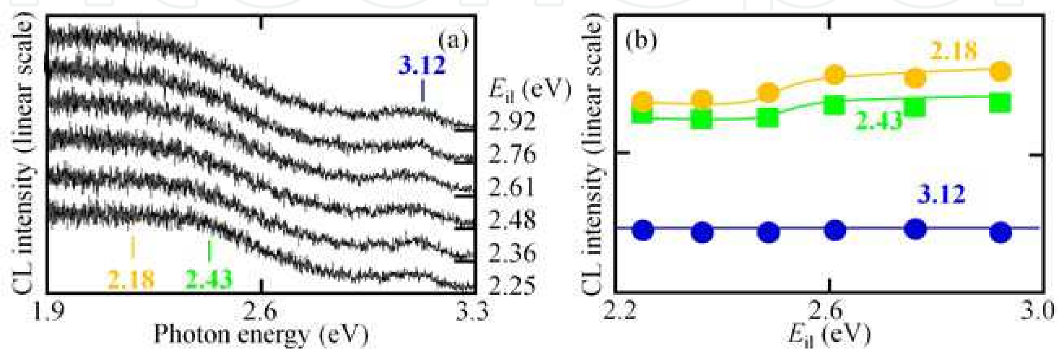

Fig. 5. (a) CL spectra after the illumination of a light with the photon energy E_{il} as in Fig. 4. (b) The CL intensity at 3.12, 2.43, or 2.18 eV vs E_{il}. (Ohno et al, 2009b). Copyright Wiley-VCH Verlag GmbH & Co. KGaA. Reproduced with permission

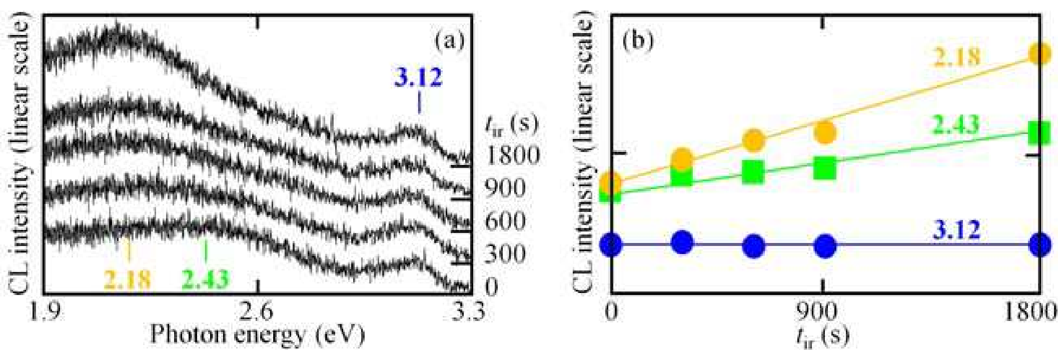

Fig. 6. (a) CL spectra after the irradiation of electrons, with flux of 5×10^{17} e mm^{-2} s^{-1} at temperature of 120 K, for the irradiation time t_{ir}. (b) The CL intensity at 3.12, 2.43, or 2.18 eV vs t_{ir}. (Ohno et al, 2009b). Copyright Wiley-VCH Verlag GmbH & Co. KGaA. Reproduced with permission

It is theoretically expected that a 60° dislocation in wurtzite GaN, which is similar to ZnO in the band gap energy, form a defect level 0.3 eV (~$0.09E_g$) above the valence band edge (Blumenau et al, 2003), and the emission due to the corresponding level is proposed (Albrecht et al, 2002). Similar emission bands related to dislocations with photon energy E_L are also observed in a wurtzite II-VI compound of CdS (Negrii & Osipyan, 1978) and another compounds with the zinc blende structure such as ZnSe (Hilpert et al, 2000), ZnTe (Naumov et al, 1993), CdTe (Shreiber et al, 1999) and GaAs (Fravacque et al, 1989), even though the dislocations are dissociated, and it is proposed that the origin of the emission bands is 90° dislocations with a defect level of ΔE ~ $10^{-1}E_g$ (Table 1). Those results suggest

that a 60° complete dislocation in ZnO is dissociated into a pair of a 90° partial dislocation and a 30° one, with a narrow separation which is difficult to observe with a conventional TEM technique, and the 90° partial dislocation would induce the 3.1 eV emission.

	structure	E_g [eV]	E_L [eV]	ΔE [eV]	$\Delta E/E_g$	model
GaN	wurtzite	3.5	2.9	0.3	0.086	60° or 90° partials
ZnO	wurtzite	3.44	3.100	0.3	0.087	90° partials with point defects?
ZnSe	zinc blende	2.82	2.61	0.22	0.078	Se(g) 90° partials
CdS	wurtzite	2.58	2.430 2.439 2.447	0.153 0.144 0.136	0.059 0.056 0.053	?
ZnTe	zinc blende	2.39	2.185 2.148	0.21 0.24	0.088 0.100	Te(g) 90° partials?
CdTe	zinc blende	1.61	1.48	0.13	0.081	Te(g) 90° partials
GaAs	zinc blende	1.52	1.13	<0.2	<0.132	As(g) 90° partials

Table 1. Emission bands related to dislocations

Figure 7 summarizes the atomistic structure of dislocations on a basal plane introduced at elevated temperatures, proposed in this ZnO work. 90° partial dislocations in the dissociated 60° dislocations would form a defect level of 0.3 eV depth acting as radiative recombination center, while the screw and edge dislocations form a defect level near the mid gap acting as non-radiative recombination center, similar to wurtzite GaN (Albrecht et al, 2002).

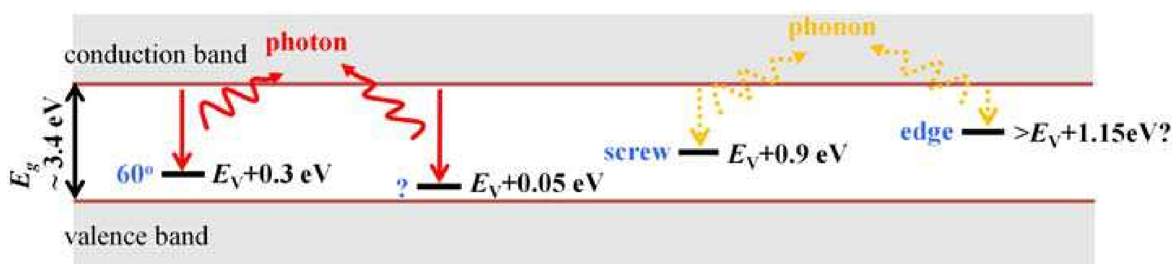

Fig. 7. A schematic view of the defect levels of misfit dislocations in ZnO

Misfit dislocations in ZnO introduced at elevated temperatures do not influence the emissions except the dislocation-related emissions, as in Fig. 2a. On the other hand, almost all emissions in ZnO are suppressed due to the introduction of misfit dislocations at room temperature (Coleman et al, 2006, Takkouk et al, 2005). Since those dislocations are similar in type, the atomistic structure of a dislocation would be modified at elevated temperatures, presumably due to an interaction of the dislocation with point defects. Indeed, a dislocation involving point defects is the candidate for the 3.1 eV emission band (Ohno et al, 2008b). Also, the intensity of the green (2.43 eV) and yellow (2.18 eV) emissions, associated with O- and Zn-vacancies (Zhao et al, 2005), varies when dislocations modify their structure via their glide (Figs. 5 and 6). This characteristic of ZnO may be an advantage over GaN, since all emissions in GaN are suppressed when dislocations are introduced even at elevated temperatures (Yonenaga et al, 2006), as well as at room temperature. (Kucheyev et al, 2000).
The interaction of dislocations with point defects is a key to elucidate the influence of dislocations on the optoelectronic properties in ZnO. In order to understand the properties

at an atomistic level, it is needed to determine an individual dislocation with a higher spatial resolution, as well as with a high spectral resolution. Near-field optical measurements in a TEM (Fig. 8) will be a unique technique to reveal the subject.

Fig. 8. A preliminary result for in-situ examination of a photo-induced glide of an individual dislocation in ZnO. TEM images of the screw dislocation indicated with the arrowhead in (a); before (a), under (b), and after (c) the illumination of a near-field light with photon energy of 2.41 eV. The broken curve in (c) indicates the dislocation line before the illumination. (Ohno, 2010a)

It is shown that transmission electron microscopy under light illumination is available to determine quantitatively the defect levels acting as non-radiative, as well as radiative, recombination centers, with a high spatial resolution. By means of this technique, combined with another in-situ techniques such as environmental TEMs (e.g., Yoshida et al, 2008, 2009) and in-situ electrifying (e.g., Nogami et al, 2009, Kohno et al, 2009), the dynamic properties of nanostructures and defects under electronic excitation will be determined.

3.2 Quantum nanostructures in middle gap semiconductors

After the successful fabrication of quantum wells based on middle gap III-V compound semiconductors including AlGaAs, around 1970, various kinds of quantum nanostructures have been fabricated. For example, by using the differences in the surface migration of adatoms and using the Stranski-Krastanov growth, quantum wires and quantum dots have been self-organized. Also, by means of modern crystal-growth techniques such as metal-organic chemical-vapor deposition and molecular-beam epitaxy, superlattices based on periodic changes of either material compositions or doping patterns have been grown. Such quantum nanostructures have potentials for enhancing the device performance, and also their electron confinement produces quantum electronic states which provide an important system for fundamental physics.

Recently, superlattices based on periodic changes of crystal directions, i.e., twinning superlattices (Ikonic et al, 1993), have been proposed in III–V (Xiong & Eklund, 2006, Ohno et al, 2007b, Algra et al, 2008, Bao et al, 2008), II-VI (Ikonic et al, 1996), and VI (Hibino et al, 1998, Fissel et al, 2006) semiconductors and in metals (e.g., Kobayashi & Uchihashi, 2010). It is expected that they can offer as much versatility in tailoring the miniband structure as there exists in heterostructure-based superlattices (e.g., Ikonic et al, 1993, Nakamura & Natori, 2006). In this subsection, the optoelectronic properties of twinning nanostructures self-organized in indirect gap $Al_{0.5}Ga_{0.5}As$ epilayers, revealed by CL spectroscopy in a TEM, are reviewed.

An $Al_{0.5}Ga_{0.5}As$ epilayer without extended defects is traditionally grown on a substrate that is flat and electrically neutral; the substrate is oxidized intentionally, to form a flat interface between the oxide and the substrate, and the oxide is then removed by the annealing in an As atmosphere, for fear of the sublimation of As atoms on the substrate. On the other hand, when a substrate is not treated the pretreatments, multiple twin boundaries are induced on

the substrate; the boundaries are induced in an epilayer grown on a rough As-deficient surface (Ohno et al, 2008c). Twin boundaries of Σ3 type are formed on (111) and (1̲1̲1) (Fig. 9). No compositional fluctuation is detected around the boundaries, indicating that heterostructures, such as $Al_xGa_{1-x}As/Al_yGa_{1-y}As$ superlattices and impurity agglomerates, are not self-organized around the boundaries.

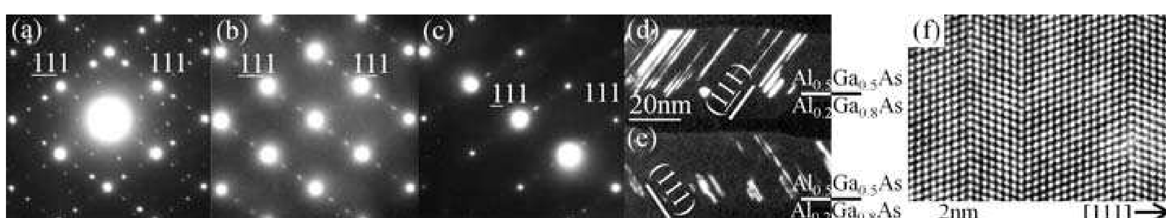

Fig. 9. Diffraction patterns of a twinned $Al_{0.5}Ga_{0.5}As$ epilayer taking along (a) [1̲10], (b) [011], and (c) nearly [01̲1]. TEM images taking with a twin spot at (d) 1/3, 1/3, 5/3 and (e) 1̲/3, 1̲/3, 5/3. (f) A high-resolution TEM image of twin boundaries. (Ohno et al, 2007b)

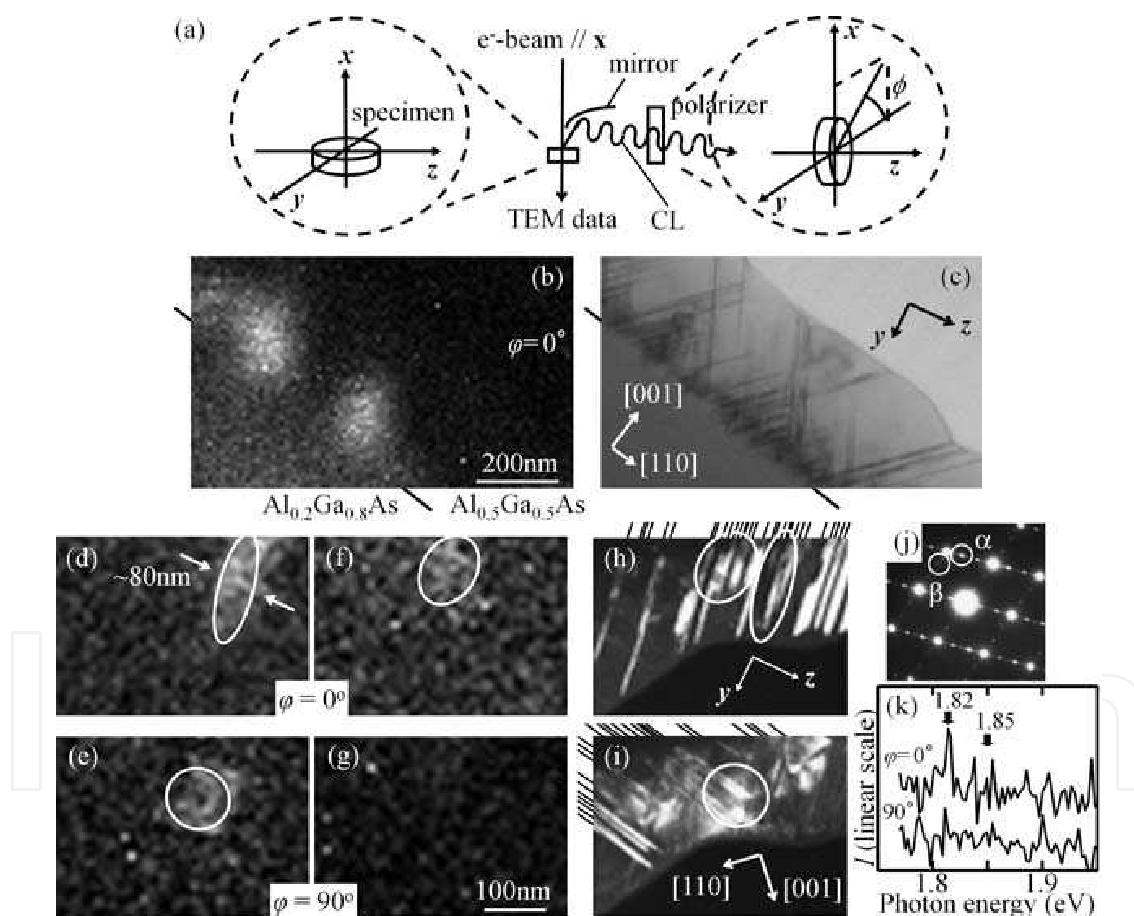

Fig. 10. (a) The experimental setup for polarized CL spectroscopy. (b) A panchromatic CL intensity map and (c) the corresponding bright-field TEM image of a twinned $Al_{0.5}Ga_{0.5}As$ epilayer grown on an $Al_{0.2}Ga_{0.8}As$. (d)-(g) Monochromatic CL intensity maps, and (h)-(i) the corresponding dark-field TEM images in which the locations of boundaries are indicated with the solid lines. The photon energy of the CL light is; (d, e) 1.82 eV or (f, g) 1.85 eV. ϕ = (d, f) 0° or (e, g) 90°. (h) or (i) is, respectively, taken with a twin spot of α or β in (j). (k) Polarized CL spectra for ϕ = 0° and 90° from the square area of Fig. (h). (Ohno et al, 2007b)

CL mapping measurements reveal that (Ohno et al, 2007b), a CL light is emitted from a twinned layer, and the intensity is stronger in comparison with the band-to-band emission in direct-gap $Al_{0.2}Ga_{0.8}As$ (Figs. 10b-10c), even though the layer is an indirect gap semiconductor. A CL light is emitted from an area in which many parallel boundaries are arranged at similar intervals of nanometer length, and no CL light is detected in the other areas (Figs. 10d-10i).

The distribution of the boundaries in a light source is characterized with the intervals between the nearest-neighbor boundaries and the distribution function of boundaries $g(l)$ (Ohno, 2010b). $g(l)$ is defined as the number of boundaries in the range of l to $l+\Delta l$ with the origin at a boundary divided by the number of boundaries N, similar to a distribution function for an extended defect (Ohno et al, 2007a): $g(l) = 1/N\ \Sigma^{N}_{i=1} n(l)/\Delta l$ in which $n(l)$ is the number of boundaries in the range of l to $l+\Delta l$ for the i-th reference boundary, l is the distance from the i-th reference boundary. Figure 11 shows an analysis of a light source, indicated with α in Fig. 11b. There is no translational symmetry in the arrangement of the boundaries, even though the intervals are much the same (Fig. 11c). However, they do not distribute randomly but orderly in a short range. There are three peaks arranged at similar intervals (peaking at the intervals of 2–5, 7–9 and 12–14 nm) in the distribution function for the ($\underline{1}11$) boundaries (Fig. 11e). Therefore, four or more ($\underline{1}11$) boundaries are arranged with the period of about 4 nm. Similar results are obtained at the areas from which a monochromatic CL light is emitted.

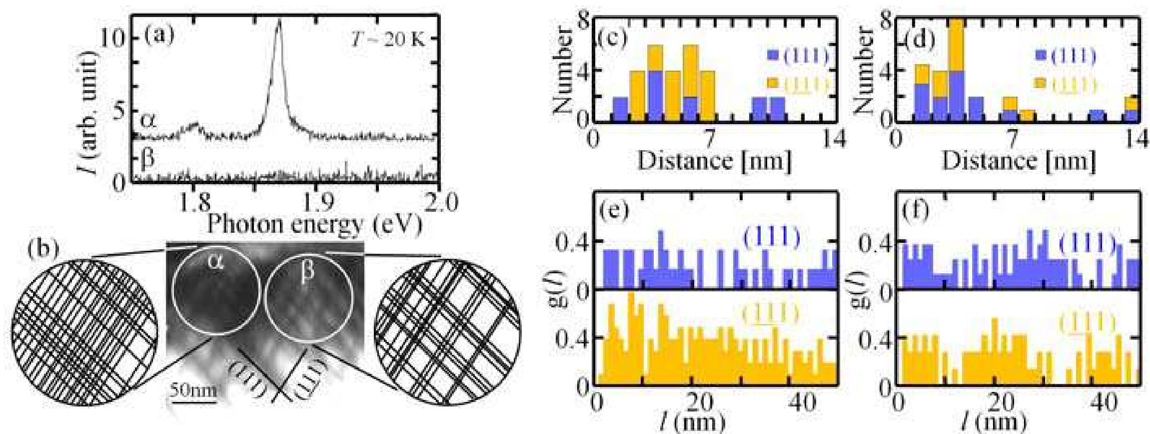

Fig. 11. (a) CL spectra obtained from the encircled areas α and β in (b) [the insets in (b) show the locations of the boundaries in the areas]. (c) or (d), respectively, shows the histogram of the intervals between the nearest-neighbor boundaries in α or β. (e) or (f), respectively, shows the distribution function of boundaries in α or β. (Ohno, 2010b)

The intensity profile of a CL light emitted from a set of parallel boundaries vs the photon energy is fitted with a Lorentz function (e,g., Fig. 11a), and the half-width at half-maximum (5–6 meV) is narrower in comparison with the band-to-band emission in direct-gap $Al_{0.2}Ga_{0.8}As$ (9–10 meV) and with an impurity emission (about 20 meV). The CL light is polarized parallel to the boundaries (Figs. 10d-10i, Fig. 12), and the photon energy increases with decreasing the interval of the boundaries. Those results indicate that a light source is a set of parallel twin boundaries ordered in a short range.

By means of temperature T-dependent CL spectroscopy (Ohno, 2010b), the energy level induced by ordered boundaries is determined (Fig. 13). The intensity of a CL light with the photon energy of E_L, I can be fitted with a function: $I(T) = I_0/[1 + C\exp(\Delta E/kT)]$ where ΔE is

the activation energy for the thermal quenching process and I_0 or C is a constant (Holtz et al, 1985). ΔE for a CL light due to ordered boundaries is higher in comparison with bound excitons, and it increases with decreasing E_L. The estimated energy is close to the difference between the band gap energy E_g and E_L, indicating that the light is emitted via an electronic transition between an energy band and a defect level associated with the boundaries; thermal escape of the carriers trapped in the level is responsible for the quenching.

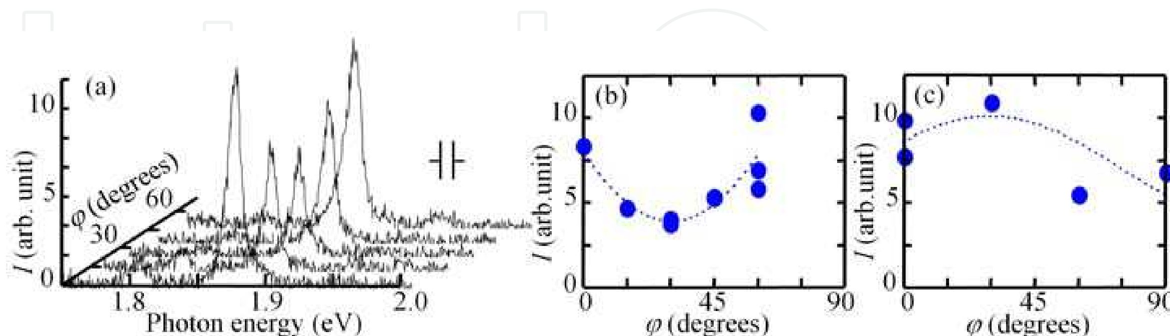

Fig. 12. (a) Polarized CL spectra for different ϕ obtained from α in Fig. 11b. The experimental setup is similar to that in Fig. 10a, and the specimen is set so that the z axis is parallel to [001]. The CL intensity I vs ϕ; the z axis is parallel to (b) [001] or (c) [110] (Ohno et al, 2007b)

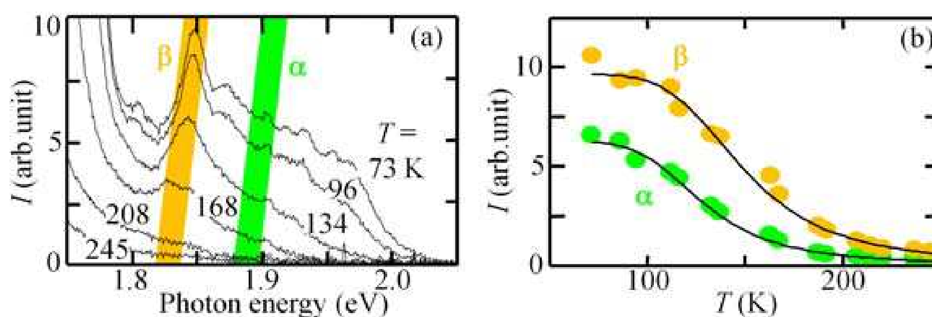

Fig. 13. (a) CL spectra obtained at various temperatures T. (b) T-dependence of the CL intensity for the emission line α and that for β in (a). (Ohno, 2010b)

Electron flux-dependent CL spectroscopy reveals that (Ohno et al, 2007c), the photon energy of a CL light due to a set of ordered boundaries is independent of electron flux. The intensity obeys a power law (Schmidt et al, 1992), and the power α is about 2.0. These results indicate that the CL light is emitted via a band-to-band electronic transition, rather than a donor–acceptor pair recombination ($\alpha < 1$) and an excitonic transition ($1 < \alpha < 2$).

Figure 14 shows the energy diagram based on a twinning superlattice theory (Ikonic et al, 1993). Suppose a twinning superlattice structure, which forms a narrow miniband whose energy is lower than the energy at the conduction band edge, is embedded in the indirect gap $Al_{0.5}Ga_{0.5}As$ crystal. According to the model, an intense monochromatic CL light with photon energy E_L, polarized parallel to the boundaries, is emitted via the direct transition between the miniband and the valence band. The thermal escape of electrons from the miniband into the conduction band in the adjacent $Al_{0.5}Ga_{0.5}As$ crystal is responsible for the quenching of the CL emission, and the activation energy for the quenching ΔE is $E_g - E_L$.

It is shown that CL spectroscopy in a TEM is available for the quantitative analyses of the optoelectronic and structural properties of nanostructures with a high spatial resolution (higher than about 80 nm as in Fig. 10d). The technique will be applied to explore novel

nanostructures and defects with useful optoelectronic functions, as well as to assess the functions at an atomistic level, inside semiconductors.

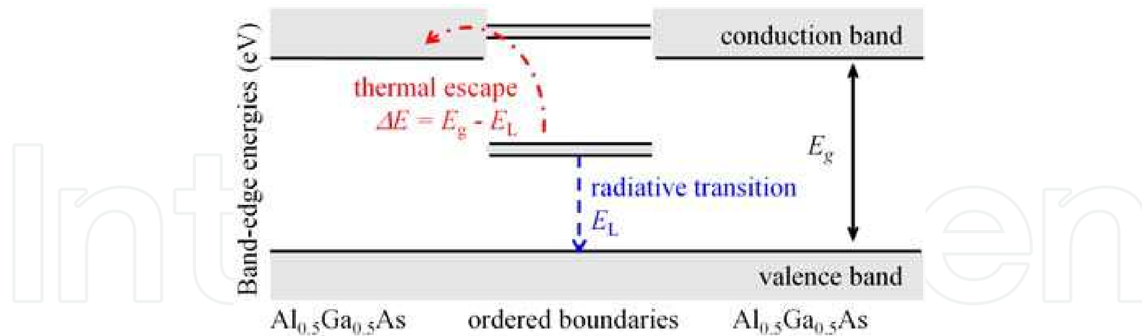

Fig. 14. A schematic view of band-edge energies for an ordered boundaries embedded in an $Al_{0.5}Ga_{0.5}As$ layer in which no twin boundary exists

3.3 Silicon and related materials as optoelectronic materials

Si and related materials are still the most important semiconductor for various kinds of photovoltaic and electronic devices. However, small numbers of the optical assessments have been performed in TEM since Si is an indirect-gap semiconductor. Even though 60° and Lomer-Cottrell dislocations are believed to act as radiative recombination center (Higgs et al, 1992, Sekiguchi & Sumino, 1996), they have not been determined in TEM. Some preliminary optical measurements for Si nanostructures which emit visible light, such as porous-Si (Itoh et al, 1996) and Si nanowires (Ozaki et al, 1998, 2005, Kohno et al, 2004), have been performed in a TEM. With a recent progress in optical measurement systems used in near-infrared region, optoelectronic properties in Si including nanostructures and extended defects, which would be modified by the interactions with point defects (e.g., Inoue et al, 2008, 2009, Ohno et al, 2009a, 2010), will be elucidated at an atomistic level.

4. Concluding remarks

In-situ optical measurements in TEM are powerful and unique techniques to examine the atomistic structures of small regions inside materials, with an extremely high spectral resolution. This in-situ technique in TEM will be applied permanently to discover and assess various novel nanomaterials.

5. Acknowledgements

This work was partially supported by the Ministry of Education, Culture, Sports, Science, and Technology, Japan, Grant-in-Aid for Scientific Research (B) #19310072 (2007–2009) and for Scientific Research on Priority Areas #21016002 (2009-2010), and the Nano-Materials Functionality Creation Research Project in IMR, Tohoku University.

6. References

Akiba, K.; Yamamoto, N.; Grillo, V.; Genseki, A. & Watanabe, Y. (2004). Anomalous temperature and excitation power dependence of cathodoluminescence from InAs quantum dots. *Phys. Rev. B*. Vol. 70, No. 16, pp. 165322/1-9.

Albrecht, M.; Strunk, H. P.; Weyher, J. L.; Grzegory, I.; Porowski, S. & Wosinski, T. (2002). Carrier recombination at single dislocations in GaN measured by cathodo-luminescence in a transmission electron microscope. *J. Appl. Phys.* Vol. 92, No. 4, pp. 2000-2005.

Albrecht, M.; Weyher, J. L.; Lucznic, B.; Grzegory, I. & Porowski, S. (2008). Nonradiative recombination at threading dislocations in *n*-type GaN: Studied by cathode-luminescence and defect selective etching. *Appl. Phys. Lett.* Vol. 92, No. 23, pp. 231909/1-3.

Algra, R. E.; Verheijen, M. A.; Borgstrom, M. T.; Feiner, L. F.; Immink, G.; van Enckevort, W. J. P.; Vlieg, E. & Bakkers, E. P. A. M. (2008). Twinning superlattices in indium phosphide nanowires. *Nature.* Vol. 436, No. 7220, pp.369-372.

Bagnall, D. M.; Chen, Y. F.; Zhu, Z.; Yao, T.; Shen, M. Y. & Goto, T. (1998). High temperature excitonic stimulated emission from ZnO epitaxial layers. *Appl. Phys. Lett.* Vol. 73, No. 8, pp. 122077/1-3.

Bao, J.; Bell, D. C.; Capasso, F.; Wagner, J. B.; Matensson, T.; Tragardh, J. & Samuelson, L. (2008). Optical properties of rotationally twinned InP nanowires heterostructures. *Nano Lett.* Vol. 8, No. 3, pp. 836-841.

Blumenau, A. T.; Fall, C. J.; Elsner, R.; Jones, R.; Heggie, M. I. & Frauenheim, T. (2003). A theoretical investigation of dislocations in cubic and hexagonal gallium nitride. *Phys. Stat. Sol. (c).* Vol. 0, No. 6, pp. 1684-1709.

Bonard, J. M.; Ganiere,J. D.; Vanzetti, L.; Paggel, J. J.; Sorba, L. & Franciosi, A. (1998). Combined transmission electron microscopy and cathodoluminescence studies of degradation in electron-beam-pumped $Zn_{1-x}Cd_xSe/ZnSe$ blue-green lasers. *J. Appl. Phys.* Vol. 84, No. 8. pp. 1263-1273.

Cheng, Y. M.; Herrick, R. W.; Petroff, P. M.; Hibbsbrenner, M. K. & Morgan, R. A. (1995). Degradation studies of proton-implanted vertical cavity surface emitting Lasers. *Appl. Phys. Lett.* Vol. 67, No. 12. pp. 1648-1650.

Coleman, V. A.; Bradby, J. E.; Jagadish, C. & Phillips, M. R. (2006). Observation of enhanced defect emission and excitonic quenching from spherically indented ZnO. *Appl. Phys. Lett.* Vol. 89, No. 8, pp. 082102/1-3.

Donolato, C. & Venturi, P. (1982). Influence of the generation distribution on the calculated EBIC contrast of line defects. *Phys. Stat. Sol. (a)* Vol. 73, No. 2, pp. 377-387.

Everhart, T. E. & Hoff, P. H. (1971). Determination of kilovolt electron energy dissipation vs penetration distance in solid materials. *J. Appl. Phys.* Vol. 42, No. 13, pp. 5837-5846.

Fissel, A.; Bugiel, E.; Wang, C. R. & Osten, H. J. (2006). Formation of Si twinning-superlattice: First step toward Si polytype growth. *Mater. Sci. Eng. B.* Vol. 134, No. 2-3, pp. 138-141.

Farvacque, J. L.; Vignaud, D.; Depraetere, E.; Sieber, B. & Lefebvre, A. (1989). Electrical and optical properties of dislocations in GaAs. *Inst. Phys. Conf. Ser.* Vol. 104, pp. 141-150.

Goldstein, J. I. (1979). Principles of thin film X-ray microanalysis. In.: *Introduction to Analytical Electron Microscopy*, Ed. Hren, J. J.; Goldstein, J. I. & Joy, D. C. pp. 83-120, Plenum Press, ISBN 0-306-40280-7, New YorK.

Graham, R. J.; Shaapur, F.; Kato, Y. & Stoner, B. R. (1994). Imaging of boron dopant in highly oriented diamond films by cathodoluminescence in a transmission electron microscope. *Appl. Phys. Lett.* Vol. 65, No. 3, pp. 292-294.

Hayazawa, N.; Tarun, A.; Inouye, Y. & Kawata, S. (2002). Near-field enhanced Raman spectroscopy using side illumination optics. *J. Appl. Phys.* Vol. 92, No. 12, pp. 6983-6986.

Henderson, B. & Imbusch, G. F. (1989). *Optical Spectroscopy of Inorganic Solids*, Clarendon Press, ISBN 0-19-851372-0, Oxford. pp. 315-386.

Hibino, H.; Sumitomo, K. & Ogino, T. (1998). Twinned epitaxial layers formed on Si(111) √3x√3-B. *J. Vac. Sci. Technol. A.* Vol. 16, No. 3, pp. 1934-1937.

Higgs, V.; Lightowlers, E. C. & Tajbakhsh, S. (1992). Cathodoluminescence imaging and spectroscopy of dislocations in Si and $Si_{1-x}Ge_x$ alloys. *Appl. Phys. Lett.* Vol. 61, No. 9, pp. 1087-1089.

Hilpert, U.; Schreiber, J.; Worschech, L.; Horing, L.; Ramsteiner, M.; Ossau, W. & Landwehr, G. (2000). Optical characterization of isolated Se(g)-type misfit dislocations and their influence on strain relief in thin ZnSe films. *J. Phys. Condens. Matter.* Vol. 12, No. 49, pp. 10169-10174.

Holt, D. B. & Napchan, E. (1994). Quantitation of SEM EBIC and CL signals using Monte Carlo electron-trajectory simulations. *Scanning.* Vol. 16, No. 2, pp. 78-86.

Holtz, P. O.; Monemar, B. & Lozykowski, H. J. (1985). Optical-properties of Ag-related centers in bulk ZnSe. *Phys. Rev. B.* Vol. 32, No. 2, pp. 986–996.

Hutchinson, H. J. & Myhajlenko, S. (1984). The cathodoluminescence study of recombination behavior at dislocations in indium-phosphide. *Philos. Mag. B.* Vol. 50, No. 4, pp. L49-L53.

Ikonic, Z.; Srivastava, G. P. & Inkson, J. C. (1993). Electronic properties of twin boundaries and twinning superlattices in diamond-type and zinc-blende-type semiconductors. *Phys. Rev. B.* Vol. 48, No. 23, pp. 17181-17193.

Ikonic, Z.; Srivastava, G. P. & Inkson, J. C. (1996). Electronic structure of natural self-organized $PbS-Bi_2S_3$ twinning superlattices. *Phys. Rev. B.* Vol. 55, No. 15, pp. 9286-9289.

Ino, N. & Yamamoto, N. (2008). Low temperature diffusion length of excitons in gallium nitride measured by cathodoluminescence technique. *Appl. Phys. Lett.* Vol. 93, No. 23, pp. 232103/1-3.

Inoue, K.; Yano, F.; Nishida, A.; Takamizawa, H.; Tsunomura, T.; Nagai, Y. & Hasegawa, M. (2009). Dopant distribution in gate electrode of *n*- and *p*-type metal-oxide-semiconductor field effect transistor by laser-assisted atom probe. *Appl. Phys. Lett.* Vol. 95, No. 4, pp. 043502/1-3.

Inoue, K.; Yano, F.; Nishida, A.; Tsunomura, T.; Toyama, T.; Nagai, Y. & Hasegawa, M. (2008). Three dimensional characterization of dopant distribution in polycrystalline silicon by laser-assisted atom probe. *Appl. Phys. Lett.* Vol. 93, No. 13, pp. 133507/1-3.

Inouye, Y. & Kawata, S. (1994). Near-field scanning optical microscope with a metallic probe tip. *Opt. Lett.* Vol. 19, No. 3, pp. 159-161.

Ishikawa, K.; Yamamoto, N.; Tateno, K. & Watanabe, Y. (2008). Characterization of individual GaAs /AlGaAs self-standing nanowires by cathodoluminescence technique using transmission electron microscope. *Jpn. J. App. Phys.* Vol. 47, No. 8, pp. 6596-6600.

Itoh, M.; Yamamoto, N.; Takemoto, K. & Nittono, O. (1996). Cathodoluminescence imaging of n-type porus silicon. *Jpn. J. Appl. Phys.* Vol. 35, No. 8, pp. 4182-4186.

Jakubowicz, A. (1986). Theory of cathodoluminescence contrast from localized defects in semiconductors. *J. Appl. Phys.* Vol. 59, No. 6, pp. 2205-2209.

Kikkawa, J.; Takeda, S.; Sato, Y. & Terauchi, M. (2007). Enhanced direct interband transitions in silicon nanowires studied by electron energy-loss spectroscopy. *Phys. Rev. B.* Vol. 75, No. 24, pp. 245317/1-5.

Kobayashi, K. & Uchihashi, T. (2010). Electronic states of Ag thin films with a laterally periodic insertion of stacking faults. *Phys. Rev. B.* Vol. 81, No. 15, pp. 155418/1-12.

Kohno, H.; Mori, Y.; Ichikawa, S.; Ohno, Y.; Yonenaga, I. & Takeda, S. (2009). Transformation of a SiC nanowire into a carbon nanotube. *Nanoscale.* Vol. 1, No. 3, pp. 344-346.

Kohno, H.; Yoshida, H.; Ohno, Y.; Ichikawa, S.; Akita, T.; Tanaka, K. & Takeda, S. (2004). Formation of silicon/silicide/oxide nanochains and their properties studied by electron holography. *Thin Solid Films.* Vol. 464, pp. 204-207.

Kucheyev, S. O.; Bradby, J. E.; Williams, J. S.; Jagadish, C.; Toth, M.; Phillips, M. R. & Swain, M. V. (2000). Nanoindentation of epitaxial GaN films. *Appl. Phys. Lett.* Vol. 77, No. 21, pp. 3373-3375.

Maeda, K.; Suzuki, K.; Ichihara, M.; Nishiguchi, S.; Ono, K.; Mera, Y. & Takeuchi, S. (1999). Electronically induced dislocation glide motion in hexagonal GaN single crystals. *Physica B.* Vol. 273, pp. 134–139.

Maeda, K.; Suzuki, K.; Yamashita, Y. & Mera, Y. (2000). Dislocation motion in semiconducting crystals under the influence of electronic perturbations. *J. Phys.: Cond. Matter.* Vol. 12, No. 49, pp. 10079–10091.

Merano, M.; Sonderegger, S.; Crottini, A.; Collin, S.; Renucci, P.; Pelucchi, E.; Malko, A.; Baier, M. H.; Kapon, E.; Deveaud, B. & Ganiere, J. D. (2005). Probing carrier dynamics in nanostructures by picosecond cathodoluminescence. *Nature.* Vol. 438, No. 7067, pp. 479 -482.

Mitsui, T. & Yamamoto, N. (1997). Distribution of polarized-cathodoluminescence around the structural defects in ZnSe/GaAs(001) studied by transmission electron microscopy. *J. Appl. Phys.* Vol. 81, No. 11, pp. 7492-7496.

Mitsui, T.; Yamamoto, N.; Tadokoro, T. & Ohta, S. (1996). Cathodoluminescence image of defects and luminescence centers in ZnS/GaAs(100). *J. Appl. Phys.* Vol. 80, No. 12, pp. 6972-6979.

Nakaji, D.; Grillo, V.; Yamamoto, N. & Mukai, T. (2005). Contrast analysis of dislocation images in TEM–cathodoluminescence technique. *J. Electron Microsc.* Vol. 54, No. 3, pp. 223-230.

Nakamura, J. & Natori, A. (2006). Dielectric discontinuity at structural boundaries in Si. *Appl. Phys. Lett.* Vol. 89, No. 5, pp. 053118/1-3.

Nakamura, S.; Mukai, T. & Senoh, M. (1994). Candela-class high-brightness InGaN/AlGaN double-heterostructure blue-light-emitting diodes. *Appl. Phys. Lett.* Vol. 64, No. 13, pp. 1687-1689.

Naumov, A.; Wolf, K.; Reisinger, T.; Stanzl, H. & Gebhardt, W. (1992). Luminescence due to lattice-mismatch defects in ZnTe layers grown by metalorganic vapor phase epitaxy. *J. Appl. Phys.* Vol. 73, No. 5, pp. 2581-2583.

Negrii, V. D. & Osipyan, Y. A. (1978). Influence of dislocations on radiative recombination processes in cadmium sulfide. *Sov. Phys. Solid State.* Vol. 20, No. 3, pp. 432-436.

Nogami, T.; Ohno, Y.; Ichikawa, S. & Kohno, H. (2009). Converting an insulating silicon nanochain to a conducting carbon nanotube by electric breakdown. *Nanotechnology.* Vol. 20, No. 33, pp. 335602/1-5.

Ohno, Y. (2005a). Polarized light emission from antiphase boundaries acting as slanting quantum wells in GaP/InP short-period superlattices. *Phys. Rev. B.* Vol. 72, No. 12, pp. 121307(R)/1-4.

Ohno, Y. (2005b). Photoinduced stress in a ZnSe/GaAs epilayer containing 90°α partial dislocations. *Appl. Phys. Lett.* Vol. 87, No. 18, pp. 181909/1-3.
Ohno, Y. (2010a). Development of an apparatus for in-situ near-field optical measurements in a transmission electron microscope, to be published.
Ohno, Y. (2010b). In-situ analysis of optoelectronic properties of twin boundaries in AlGaAs by polarized cathodoluminescence spectroscopy in a TEM. *J. Electron Microsc.* Vol. 59, No. S1, pp. S141-S147.
Ohno, Y.; Kawai, Y. & Takeda, S. (1999). Vacancy-migration-mediated disordering in CuPt-ordered (Ga, In)P studied by in situ optical spectroscopy in a transmission electron microscope. *Phys. Rev. B.* Vol. 59, No. 4, pp. 2694-2699.
Ohno, Y.; Koizumi, H.; Taishi, T.; Yonenaga, I.; Fujii, K.; Goto, H. & Yao, T. (2008a). Light emission due to dislocations in wurtzite ZnO bulk single-crystals freshly introduced by plastic deformation. *Appl. Phys. Lett.* Vol. 92, No. 1, pp. 011922/1-3.
Ohno, Y.; Koizumi, H.; Taishi, T.; Yonenaga, I.; Fujii, K.; Goto, H. & Yao, T. (2008b). Optical properties of dislocations in wurtzite ZnO single-crystals introduced at elevated temperatures. *J. Appl. Phys.* Vol. 104, No. 7, pp. 073515/1-6.
Ohno, Y.; Shoda, K.; Taishi, T.; Yonenaga, I. & Takeda, S. (2008c). Formation of multiple nanoscale twin boundaries that emit intense light in indirect-gap AlGaAs epilayers. *Appl. Surf. Sci.* Vol. 254, No. 23, pp. 7633-7637.
Ohno, Y.; Shirakawa, T.; Taishi, T. & Yonenaga, I. (2009a). Interaction of phosphorus with dislocations in heavily phosphorus doped silicon. *Appl. Phys. Lett.* Vol. 95, No. 9, pp. 091915/1-3.
Ohno, Y.; Taishi, T.; Tokumoto, Y. & Yonenaga, I. (2010). Interaction of dopant atoms with stacking faults in silicon crystals. *J. Appl. Phys.* Vol. 108, No. 7, pp. 073514/1-4.
Ohno, Y.; Taishi, T. & Yonenaga, I. (2009b). In-situ analysis of optoelectronic properties of dislocations in ZnO by TEM observations. *Phys. Stat. Sol. (a).* Vol. 206, No. 8, pp. 1904-1911.
Ohno, Y. & Takeda, S. (2002). Analysis of polarization by means of polarized cathodoluminescence spectroscopy in a TEM. *J. Electron Microsc.* Vol. 51, No. 5, pp. 281-290.
Ohno, Y & Takeda, S. (1995). A new apparatus for in-situ photoluminescence spectroscopy in a transmission electron microscope. *Rev. Sci. Instrum.* Vol. 66, No. 10, pp. 4866-4869.
Ohno, Y. & Takeda, S. (1996). Study of electron-irradiation-induced defects in GaP by in-situ optical spectroscopy in a transmission electron microscope. *J. Electron Microsc.* Vol. 45, No. 1, pp. 73-78.
Ohno, Y.; Takeda, S.; Ichihashi, T. & Iijima, S. (2007a). Fabrication of short-range ordered nanoholes on silicon surfaces by electron irradiation. *Jpn. J. Appl. Phys.* Vol. 46, No. 1, pp. 434–439.
Ohno, Y.; Yamamoto, N.; Shoda, S. & Takeda, S. (2007b). Intense monochromatic light emission from multiple nanoscale twin boundaries in indirect-gap AlGaAs epilayers, *Jpn. J. Appl. Phys.* Vol. 46, No. 35, pp. L830-L832.
Ohno, Y.; Yamamoto, N.; Taishi, T.; Yonenaga, I. & Takeda, S. (2007c). Electronic properties of nanoscale multiple twin boundaries in AlGaAs. *Physica B.* Vol. 401, pp. 270-274.
Ozaki, N.; Ohno, Y.; Kikkawa, J. & Takeda, S. (2005). Growth of silicon nanowires on H-terminated Si {111} surface templates studied by transmission electron microscopy. *J. Electron Microsc.* Vol. 54, No. S1, pp. I25-i29.

Ozaki, N.; Ohno, Y. & Takeda, S. (1998). Silicon nanowhiskers grown on a hydrogen-terminated silicon {111} surface. *Appl. Phys. Lett.* Vol. 73, No. 25, pp. 3700-3702.

Petroff, P. M.; Lang, D. V.; Logan, R. A. & Strudel, J. L. (1978). Scanning transmission electron microscopy techniques for simultaneous electronic analysis and observation defects in semiconductors. *Scanning Electron Microsc.* Vol. 1, pp. 325-332.

Petroff, P. M.; Logan, R. A. & Savage, A. (1980). Nonradiative recombination at dislocations in III-V compound semiconductors. *Phys. Rev. Lett.* Vol. 44, No. 4, pp. 287-291.

Schmidt, T.; Lischka, K. & Zulehner, W. (1992). Excitation-power dependence of the near-band-edge photoluminescence of semiconductors. *Phys. Rev. B.* Vol. 45, No. 16, pp. 8989–8994.

Schreiber, J. & Hildebrandt S. (1994). Basic dislocation contrasts in SEM-CL/EBIC on III–V semiconductors . *Mater. Sci. Eng. B*. Vol. 24, No. 1-3, pp. 115-120.

Schreiber, J.; Horing, L.; Uniewski, H.; Hildebrandt, S. & Leipner, H. S. (1999). Recognition and distribution of A(g) and B(g) dislocations in indentation deformation zones on {111} and {110} surfaces of CdTe. *Phys. Status Solidi (a)*. Vol. 171, No. 1, pp. 89–97.

Sekiguchi, T. & Sumino, K. (1996). Cathodoluminescence study on dislocation in silicon. *J. Appl. Phys.* Vol. 79, No. 6, pp. 3253-3260.

Setiawan, A.; Vashaei, Z.; Cho, M. W.; Yao, T.; Kato, K.; Sano, M.; Miyamoto, K.; Yonenaga, I. & Ko, H. J. (2004). Characteristics of dislocations in ZnO layers grown by plasma-assisted molecular beam epitaxy under different Zn/O flux ratios. *J. Appl. Phys.* Vol. 96, No. 7, pp. 1785852/1-6.

Sieber, B.; Farvacque, J. L.; Wang, J. & Steeds, J. W. (1993). 1st step of degradation mechanisms in AlGaAs/GaAs laser-like structures. *Mater. Sci. Eng. B.* Vol. 20, No. 1-2, pp. 29-32 (1993).

Sonderegger, S.; Feltin, E.; Merano, M.; Crottini, A.; Carlin, J. F.; Sachot, R.; Deveaud, B.; Grandjean, N. & Ganiere, J. D. (2006). High spatial resolution picosecond cathodoluminescence of InGaN quantum wells. *Appl. Phys. Lett.* Vol. 89, No. 23, pp. 232109/1-3.

Suzuki, K.; Ichihara, M. & Takeuchi, S. (1994). High-resolution electron microscopy of extended defects in wurtzite crystals. *Jpn. J. Appl. Phys.* Vol. 33, No. 2, pp. 1114-1120.

Suzuki, K.; Ichihara, M.; Takeuchi, S.; Nakagawa, K.; Maeda, K. & Iwanaga, H. (1984). In-situ TEM observation of dislocation-motion in II-VI compounds. *Phillos. Mag. A.* Vol. 49, No. 3, pp. 451-461.

Suzuki, K. & Takeuchi, S. (1999). Electron microscopy of dislocations introduced into GaN by plastic deformation. *Phillos. Mag. Lett.* Vol. 79, No. 7, pp. 423-428.

Takkouk, Z.; Brihi, N.; Guergouri, K. & Marfaing, Y. (2005). Cathodoluminescence study of plastically deformed bulk ZnO single crystal. *Physica B*. Vol. 366, No. 1-4, pp. 185-191.

Terauchi, M.; Koike, M.; Fukushima, K. & Kimura, A. (2010). Development of wavelength-dispersive soft X-ray emission spectrometers for transmission electron microscopes – an introduction of valence electron spectroscopy for transmission electron microscopy. *J. Electron Microsc.* Vol. 59, No. 4, pp. 251-261.

Tsukazaki, A.; Ohtomo, A.; Onuma, T.; Ohtani, M.; Makino, T.; Sumiya, M.; Ohtani, K.; Chichibu, S. F.; Fuke, S.; Segawa, Y.; Ohno, H.; Koinuma, H.& Kawasaki, M. (2005). Repeated temperature modulation epitaxy for p-type doping and light-emitting diode based on ZnO. *Nature Mater.* Vol. 4, No. 1, pp. 42-46.

Wang. J. N.; Steeds, J. W. & Hopkinson, M. (1993). Microstructure and cathodoluminescence of MBE-grown (001) $In_xGa_{1-x}P$/GaAs strained-layer heterostructures. *Semicond. Sci. Technol.* Vol. 8, No. 4, pp. 502-508.

Wang, J. N.; Steeds, J. W. & Woolf, D. A. (1992). The study of misfit dislocations in $In_xGa_{1-x}As$/GaAs strained quantum-well structures. *Phillos. Mag. A*. Vol. 65, No. 4, pp. 829-839.

Xiong, Q. & Eklund, P. C. (2006). Coherent twinning phenomena: towards twinning superlattices in III-V semiconducting nanowires. *Nano Lett.* Vol. 6, No. 12, pp. 2736-2742.

Yacobi, B. G. & Holt, D. B. (1990). *Cathodoluminescence Microscopy of Inorganic Solids,* Plenum Press, ISBN 0-306-43314-1, New York. pp. 89-120.

Yamamoto, N.; Bhunia, S. & Watanabe, Y. (2006). Polarized cathodoluminescence study of InP nanowires by transmission electron microscopy. *Appl. Phys. Lett.* Vol. 88, No. 15, pp. 153106/1-3.

Yamamoto, N.; Itoh, H.; Grillo, V.; Chichibu, S. F.; Keller, S.; Spence, J. S.; DenBaars, S. P; Mishra, U. K.; Nakamura, S. & Salviati, G. (2003). Cathodoluminescence characterization of dislocations in gallium nitride using a transmission electron microscope. *J. Appl. Phys.* Vol. 94, No. 7, pp. 4315-4319.

Yamamoto, N.; Spence, J. C. H. & Fathy, D. (1984). Cathdoluminescence and polarization studies from individual dislocations in diamond. *Philos. Mag. B*. Vol. 49, No. 6, pp. 609-629.

Yonenaga, I.; Makino, H.; Itoh, S.; Goto, T. & Yao, T. (2006). Photoluminescence properties of GaN with dislocations induced by plastic deformation. *J. Electron. Mater.* Vol. 35, No. 4, pp. 717-721.

Yonenaga, I.; Koizumi, H.; Ohno, Y. & Taishi, T. (2008). High-temperature strength and dislocation mobility in the wide band-gap ZnO: Comparison with various semiconductors. *J. Appl. Phys.* Vol. 103, No. 9, pp. 093502/1-4.

Yoshida, H.; Shimizu, T.; Uchiyama, T.; Kohno, H.; Homma, Y. & Takeda, S. (2009). Atomic-scale analysis on the role of molybdenum in iron-catalyzed carbon nanotube Growth. *Nano Lett.* Vol. 9, No. 11, pp. 3810-3815.

Yoshida, H.; Takeda, S.; Uchiyama, T.; Kohno, H. & Homma, Y. (2008). Atomic-scale in-situ observation of carbon nanotube growth from solid state iron carbide nanoparticles. *Nano Lett*. Vol. 8, No. 7, pp. 2082-2086.

Yoshida, K.; Nanbara, T.; Nozaki, T.; Hirayama, T. & Tanaka, N. (2007). In situ high-resolution transmission electron microscopy of photocatalytic reactions by excited electrons in ionic liquid. *J. Electron Microsc.* Vol. 56, No. 5, pp. 177-180.

Yoshida, K.; Nanbara, T.; Yamasaki, J. & Tanaka, N. (2006). Oxygen release and structural changes in TiO_2 films during photocatalytic oxidation. *J. Appl. Phys.* Vol. 99, No. 8, pp084908/1-8.

Yoshida, K.; Yamasaki, J. & Tanaka, N. (2004). In situ high-resolution transmission electron microscopy observation of photodecomposition process of poly-hydrocarbons on catalytic TiO_2 films. *Appl. Phys. Lett.* Vol. 84, No. 14, pp2542-2544.

Yu, P. Y. & Cardona, M. (2001). *Fundamentals od Semiconductors,* Springer, ISBN 3-540-41323-5, New York. pp. 345-426.

Zhao, Q. X.; Klason, P.; Willander, M.; Zhong, H. M.; Lu, W. E. & Yang. J. H. (2005). Deep-level emissions influenced by O and Zn implantations in ZnO. *Appl. Phys. Lett.* Vol. 87, No. 21, pp. 211912/1-3.

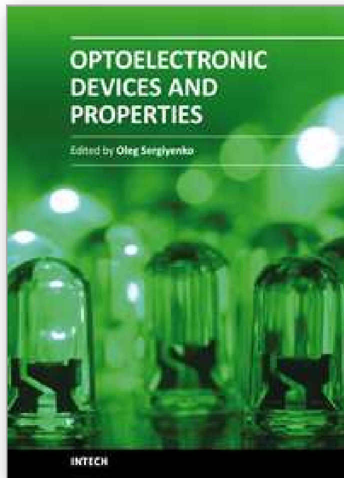

Optoelectronic Devices and Properties
Edited by Prof. Oleg Sergiyenko

ISBN 978-953-307-204-3
Hard cover, 660 pages
Publisher InTech
Published online 19, April, 2011
Published in print edition April, 2011

Optoelectronic devices impact many areas of society, from simple household appliances and multimedia systems to communications, computing, spatial scanning, optical monitoring, 3D measurements and medical instruments. This is the most complete book about optoelectromechanic systems and semiconductor optoelectronic devices; it provides an accessible, well-organized overview of optoelectronic devices and properties that emphasizes basic principles.

How to reference
In order to correctly reference this scholarly work, feel free to copy and paste the following:

Yutaka Ohno, Ichiro Yonenega and Seiji Takeda (2011). In-Situ Analysis of Optoelectronic Properties of Semiconductor Nanostructures and Defects in Transmission Electron Microscopes, Optoelectronic Devices and Properties, Prof. Oleg Sergiyenko (Ed.), ISBN: 978-953-307-204-3, InTech, Available from: http://www.intechopen.com/books/optoelectronic-devices-and-properties/in-situ-analysis-of-optoelectronic-properties-of-semiconductor-nanostructures-and-defects-in-transmi

INTECH
open science | open minds

InTech Europe
University Campus STeP Ri
Slavka Krautzeka 83/A
51000 Rijeka, Croatia
Phone: +385 (51) 770 447
Fax: +385 (51) 686 166
www.intechopen.com

InTech China
Unit 405, Office Block, Hotel Equatorial Shanghai
No.65, Yan An Road (West), Shanghai, 200040, China
中国上海市延安西路65号上海国际贵都大饭店办公楼405单元
Phone: +86-21-62489820
Fax: +86-21-62489821

© 2011 The Author(s). Licensee IntechOpen. This chapter is distributed under the terms of the Creative Commons Attribution-NonCommercial-ShareAlike-3.0 License, which permits use, distribution and reproduction for non-commercial purposes, provided the original is properly cited and derivative works building on this content are distributed under the same license.

IntechOpen

IntechOpen